studied are 1285, 1116, and 1060 cm^{-1}; these may be associated with the bending vibrations, $\delta(C_mH)$, which are insensitive to changes in core size. The empirical correlations established here allow structural conclusions to be made concerning BChl *a* ligation states; however, a more exact description of the vibrations awaits a normal coordinate calculation on BChl *a* and a more detailed compendium of model spectra.

The above correlations apply to monomeric BChl *a* RR spectra taken at or near room temperature. In a low-temperature study of BChl *a* at 77 K, all the samples that were five-coordinate oxygen and nitrogen liganded species at room temperature displayed a band A position of 1595 cm^{-1}, indicative of six-coordination at the central Mg^{2+} (data not shown). These results indicate that spectra of isolated BChl *a* taken at low *T* cannot be used to identify the room-temperature structures; i.e., the equilibrium constant for axial ligation is temperature sensitive.

Examples of monomeric BChl *a* in vivo that may be analyzed by the structural correlations presented here are: monomeric BChl *a* in the RC from *Rb. sphaeroides*[2] and monomeric B800 in the B800-850 antenna complex from *Rb. sphaeroides*[44]. The Q_y band of monomeric BChl *a* in the RC is electronically coupled to the BChl *a* "special pair" P865, and excited-state π–π^* effects have not been considered here so any structural conclusions would not be valid. However, in the oxidized state of the RC, the two monomeric BChl *a* molecules have a weaker electronic interaction with P865.[45] In this form, the Q_x absorption maxima are observed at ≈590 nm[46] and the band A frequency position of all the BChl *a* pigments appears at 1610 cm^{-1}, with downshifted acetyl stretching frequencies.[47] Therefore, we conclude that the structure of monomeric RC BChl *a* is five-coordinate, with a nitrogenous ligand and hydrogen bonding involved at the ring periphery. This is consistent with the X-ray crystal structure description of these pigments.[48]

Another monomeric BChl *a* pigment can be found in the antenna protein B800-850. The Q_x band of the B800 antenna pigment was identified at 585 nm by linear dichroism studies[44] and its band A position is at 1610 cm^{-1}.[41] The RR spectra also indicate strong interactions at the acetyl group.[41] Thus, a nitrogen ligand to BChl *a* resulting in five-coordinate Mg^{2+} and a hydrogen bond at the ring periphery is again the presumed structure. This coordination conclusion is consistent with the low-frequency RR data of Robert and Lutz[41] and with the presence of a highly conserved histidine group found in the membrane spanning region of all the purple photosynthetic bacteria antenna proteins sequenced to date.[49] We are unable to speculate about mixed-ligand structures as they are difficult to prepare in solution. Futher work on absorption and RR spectroscopy of aggregated BChl *a* model systems and a more complete study of hydrogen bonding on the spectrum of BChl *a* are being carried out in order to provide structural conclusions for additional BChl *a*–protein systems.

Acknowledgment. Isolation of BChl *a* and BPheo *a* by Constance Rose and financial support from NIH Grant GM35108 are gratefully acknowledged.

Registry No. BChl *a*, 17499-98-8; BPheo *a*, 17453-58-6.

(44) Bolt, J.; Sauer, K. *Biochim. Biophys. Acta* **1979**, *546*, 54–63.
(45) Kirmaier, C.; Holten, D.; Parson, W. *Biochim. Biophys. Acta* **1985**, *810*, 49–61.
(46) Sauer, K. *Acc. Chem. Res.* **1978**, *11*, 257–264.
(47) Zhou, Q.; Robert, B.; Lutz, M. *Biochim. Biophys. Acta* **1987**, *890*, 368–376.
(48) Allen, J. P.; Feher, G.; Yeates, T. O.; Rees, R. C.; Deisenhofer, J.; Michel, H.; Huber, R. *Proc. Natl. Acad. Sci. U.S.A.* **1986**, *83*, 8589–8593.
(49) Zuber, H. *Photochem. Photobiol.* **1985**, *42*, 821–844.

An ab Initio Study of the Reaction Pathways for $OH + C_2H_4 \rightarrow HOCH_2CH_2 \rightarrow$ Products

Carlos Sosa[†] and H. Bernhard Schlegel*[‡]

Contribution from the Department of Chemistry, Wayne State University, Detroit, Michigan 48202. *Received October 20, 1986*

Abstract: The energetically favorable reaction paths for the unimolecular decomposition of the primary addition product of $OH + C_2H_4$ have been studied with ab initio techniques. Equilibrium geometries and transition structures were fully optimized with 3-21G and 6-31G* basis sets at the Hartree–Fock level. Heats of reaction and barrier heights have been computed with Møller–Plesset perturbation theory up to fourth order, with and without annihilation of spin contamination. At the MP4 level barrier heights are lowered by 2–7 kcal/mol when the largest spin contaminant is removed. After the addition of $OH + C_2H_4$ to form the 2-hydroxyethyl radical, the most favorable reaction path (other than decomposition to reactants) is the [1,3]-hydrogen shift to form ethoxy radical followed by a dissociation into $CH_3 + CH_2O$. Other slightly higher energy paths include dissociation of ethoxy into $H + CH_3CHO$ and decomposition of the 2-hydroxyethyl radical into $H + HOCHCH_2$.

The hydroxyl radical plays an important role both in combustion processes and in atmospheric chemistry.[1] To a large extent, the fate of alkenes in the atmosphere is governed by their reaction with OH. In turn, the reaction with alkenes is an important factor controlling the atmospheric concentration of OH. These reactions are dominated by electrophilic addition,[2–19] with hydrogen abstraction occurring only at higher temperatures.[1,20,21] For the simplest alkene, ethylene, OH addition produces chemically activated 2-hydroxyethyl radical **1**, which can be collisionally stabilized, or revert to reactants, or react further to yield a variety

Scheme I

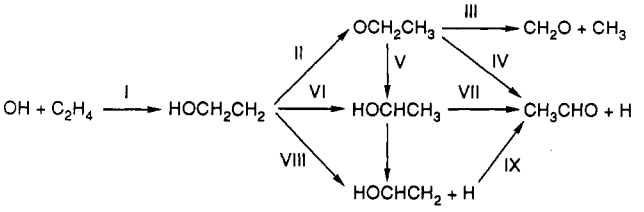

[†] Present address: Quantum Theory Project, University of Florida, Gainesville, FL 32605.
[‡] Camille and Henry Dreyfus Teacher-Scholar.

of products. Scheme I outlines some of the energetically reasonable possibilities for the decomposition of **1**.

The 2-hydroxyethyl radical can undergo a [1,3]-hydrogen shift (reaction II) to form ethoxy radical, which can fragment to formaldehyde and methyl radical (reaction III), or decompose to acetaldehyde and hydrogen (reaction IV), or isomerize to 1-hydroxyethyl radical (reaction V). Alternatively, a [1,2]-hydrogen shift (reaction VI) converts **1** to 1-hydroxyethyl radical, which can lose hydrogen (reaction VII) to form acetaldehyde. A third possibility is the loss of a β-hydrogen from **1** (reaction VIII) to yield vinyl alcohol, which can isomerize to acetaldehyde (reaction IX).

A number of studies have been carried out on the gas-phase kinetics of OH + C_2H_4.[2-19] In general, the reaction is followed by observing the disappearance of OH. However, in some studies the primary product, $HOCH_2CH_2$, and secondary products, CH_2O and CH_3CHO, have been detected by mass spectroscopy.[3,16] Similar to other hydroxyl radical plus alkene reactions, OH + C_2H_4 has a small negative Arrhenius activation energy, ca. −0.9 ± 0.3 kcal/mol.[2,14,17,19]

Some spectroscopic data are available for the individual reactive intermediates indicated in Scheme I. ESR has been used to characterize 1-hydroxyethyl radical CH_3CHOH, 2-hydroxyethyl radical $HOCH_2CH_2$, and ethoxy radical C_2H_5O.[22-27] Ethoxy radical has also been studied by laser-induced fluorescence.[28,29] Microwave spectroscopy and matrix-isolation techniques have been used to observe vinyl alcohol,[30,31] yielding the equilibrium conformation and the infrared spectrum, as well as some limited information on the isomerization to acetaldehyde, reaction IX. Studies of the decomposition of ethoxy radical in the gas phase[32-34] give a barrier of 20–22 kcal/mol for reaction III. Experimental data on [1,2]- and [1,3]-hydrogen shifts in radicals (e.g., reactions II, V, and VI) are rather limited, although [1,4] and [1,5] shifts are well-known.[35] Heats of formation have been measured for CH_3CH_2O[32] and $HOCHCH_2$;[36] reasonable estimates can be made for $HOCH_2CH_2$ and CH_3CHOH.

Theoretical calculations have been carried out for many of the structures and reactions in Scheme I, or for closely related models. In previous work[37] we have investigated the barrier for reaction I using spin-projected methods and obtained good agreement with experiment. For the rearrangement of vinyl alcohol to acetaldehyde, reaction IX, Yamabe et al.[38] and Radom et al.[39] find ca. 85 kcal/mol for the activation energy and −10 to −12 kcal/mol for the heat of reaction. Such a high barrier clearly indicates that reaction IX is energetically inaccessible in the OH + C_2H_4 system. Our studies of H + C_2H_3F[40,41] and H + C_2H_4[42] serve as models for reaction VIII. The H + CH_2O[42-45] system provides an example for reactions IV and VII. Hydrogen [1,2] shifts have been studied in CH_3O[43-45] and CH_3CH_2,[46] analogues of reactions V and VI. The conformational behavior of XCH_2CH_2 and CH_3CHX radicals has also been investigated theoretically.[23,47] Melius, Binkley, and Koszykowski[48] have studied the energetics of a number of OH addition reactions, including OH + C_2H_4 → $HOCH_2CH_2$ → products, using the BAC-MP4 approach (fourth order Møller–Plesset with bond additivity corrections). These calculations and the present work are in close agreement, even though quite different approaches are used to correct the calculated MP4 energies.

Method

Ab initio molecular orbital calculations were performed with the GAUSSIAN 82 system of programs.[49] The restricted Hartree–Fock method (RHF) was used for closed-shell systems and the unrestricted Hartree–Fock method (UHF) for open-shell systems.[50] The geometries for all stationary points were fully optimized with analytical gradient methods[51] at the Hartree–Fock level using split-valence (3-21G) and split-valence plus polarization (6-31G*) basis sets.[52,53] Electron correlation energy was cal-

(1) (a) *Combustion Chemistry*; Gardiner, W. C., Jr., Ed.; Springer-Verlag: New York, 1984. (b) Hucknall, D. J. *Chemistry of Hydrocarbon Combustion*; Chapman and Hall: New York, 1985.
(2) Greiner, N. R. *J. Chem. Phys.* **1970**, *53*, 1284.
(3) Morris, E. D., Jr.; Stedman, D. H.; Niki, H. *J. Am. Chem. Soc.* **1971**, *93*, 3570.
(4) Morris, E. D., Jr.; Niki, H. *J. Phys. Chem.* **1971**, *75*, 3640.
(5) Smith, I. W. M.; Zellner, R. *J. Chem. Soc., Faraday Trans. 2* **1973**, *69*, 1617.
(6) Bradley, J. N.; Hack, W.; Hoyermann, K.; Wagner, H. G. *J. Chem. Soc., Faraday Trans. 1* **1973**, *69*, 1889.
(7) Pastrana, A. V.; Carr, R. W., Jr. *J. Phys. Chem.* **1975**, *79*, 765.
(8) Cox, R. A. *Int. J. Chem. Kinetics Symp.* **1975**, *1*, 379.
(9) Gordon, S.; Mulac, N. A. *Int. J. Chem. Kinetics Symp.* **1975**, *1*, 289.
(10) Davis, D. D.; Fischer, S.; Schiff, R.; Watson, R. T.; Bollinger, W. *J. Chem. Phys.* **1975**, *63*, 1707.
(11) Howard, C. J. *J. Chem. Phys.* **1976**, *65*, 4771.
(12) Lloyd, A. C.; Darnall, K. R.; Winer, A. M.; Pitts, J. N., Jr. *J. Phys. Chem.* **1976**, *80*, 789.
(13) Overend, R.; Paraskevpoulos, G. *J. Chem. Phys.* **1977**, *67*, 674.
(14) Atkinson, R.; Perry, R. A.; Pitts, J. N., Jr. *J. Chem. Phys.* **1977**, *66*, 1197.
(15) Atkinson, R.; Darnall, K. R.; Lloyd, A. C.; Winer, A. M.; Pitts, J. N., Jr. *Adv. Photochem.* **1979**, *11*, 375.
(16) Bartels, M.; Hoyermann, K.; Sievert, R. *Nineteenth Symp. (Int.) Combust.* **1982**, 61.
(17) Tully, F. P. *Chem. Phys. Lett.* **1983**, *96*, 148.
(18) Klein, Th.; Barnes, I.; Becker, K. H.; Fink, E. H.; Zabel, F. *J. Phys. Chem.* **1984**, *88*, 5020.
(19) Zellner, R.; Lorenz, K. *J. Phys. Chem.* **1984**, *88*, 984.
(20) Bradley, J. N.; Capey, W. D.; Fair, R. W.; Pritchard, D. K. *Int. J. Chem. Kinet.* **1976**, *8*, 549.
(21) Westbrook, C. K.; Dryer, F. L.; Schug, K. P. *Nineteenth Symp. (Int.) Combust.* **1982**, 153.
(22) (a) Dobbs, A. J.; Gilbert, B. C.; Norman, R. O. C. *J. Chem. Soc., Perkin Trans. 2* **1972**, 786. (b) Dobbs, A. J.; Gilbert, B. C.; Norman, R. O. C. *J. Chem. Soc. (A)* **1971**, 124.
(23) Cirelli, G.; Ha, T.-K.; Meyer, R.; Gunthard, Hs. H. *Chem. Phys.* **1982**, *72*, 15.
(24) Beckwith, A. L. J.; Norman, R. O. C. *J. Chem. Soc. (B)* **1969**, 400.
(25) (a) Kawamura, T.; Edge, D. J.; Kochi, J. K. *J. Am. Chem. Soc.* **1972**, *94*, 1752. (b) Edge, D. J.; Kochi, J. *J. Am. Chem. Soc.* **1972**, *94*, 6485, 7695.
(26) Krusik, P. J.; Meakin, P.; Jesson, J. P. *J. Phys. Chem.* **1971**, *75*, 3438.
(27) (a) Livingston, R.; Zeldes, H. *J. Chem. Phys.* **1966**, *44*, 1245. (b) Zeldes, H.; Livingston, R. *J. Chem. Phys.* **1966**, *45*, 1946.
(28) Ebata, T.; Yanagishita, H.; Obi, K.; Tanaka, I. *Chem. Phys.* **1982**, *69*, 27.
(29) Inoue, G.; Okuda, M.; Akimoto, H. *J. Chem. Phys.* **1981**, *75*, 2060.
(30) Saito, S. *Chem. Phys. Lett.* **1976**, *42*, 399.
(31) Hawkins, M.; Andrews, L. *J. Am. Chem. Soc.* **1983**, *105*, 2423.
(32) Batt, L.; Milne, R. T. *Int. J. Chem. Kinet.* **1977**, *9*, 549.
(33) Batt, L. *Int. J. Chem. Kinet.* **1979**, *11*, 977.
(34) Choo, K. Y.; Benson, S. W. *Int. J. Chem. Kinet.* **1981**, *13*, 833.
(35) Benson, S. W. *Thermochemical Kinetics*, 2nd ed.; Wiley: New York, 1976.
(36) Holmes, J. L.; Lossing, F. P. *J. Am. Chem. Soc.* **1982**, *104*, 2648.
(37) Sosa, C.; Schlegel, H. B. *J. Am. Chem. Soc.* **1987**, *109*, 4193.
(38) Yamabe, T.; Koizumi, M.; Yamashita, K.; Tachibana, A. *J. Am. Chem. Soc.* **1984**, *106*, 2255.
(39) (a) Bouma, W. J.; Poppinger, D.; Radom, L. *J. Am. Chem. Soc.* **1977**, *99*, 6443. (b) Bouma, W. J.; Radom, L.; Rodwell, W. R. *Theor. Chim. Acta* **1980**, *56*, 149.
(40) Schlegel, H. B. *J. Phys. Chem.* **1982**, *86*, 4878.
(41) Schlegel, H. B.; Bhalla, K. C.; Hase, W. L. *J. Phys. Chem.* **1982**, *86*, 4883.
(42) Sosa, C.; Schlegel, H. B. *Int. J. Quantum Chem.* **1986**, *29*, 1001; *30*, 155.
(43) Saebø, S.; Radom, L.; Schaefer, H. F., III *J. Chem. Phys.* **1983**, *78*, 845.
(44) Adams, G. F.; Bartlett, R. J.; Purvis, G. D. *Chem. Phys. Lett.* **1982**, *87*, 311.
(45) Harding, L. B. In Annual Report, Theoretical Chemistry Group, Argonne National Laboratory, October 1980–September 1981.
(46) Harding, L. B. *J. Am. Chem. Soc.* **1981**, *103*, 7469.
(47) Pross, A.; Radom, L. *Tetrahedron.* **1980**, *36*, 1999.
(48) Melius, C. F.; Binkely, J. S.; Koszykowski, M. L. *8th Int. Symp. on Gas Kinetics*; Nottingham, England, 1984, and unpublished results.
(49) Binkley, J. S.; Frisch, M. J.; DeFrees, D. J.; Raghavachari, K.; Whiteside, R. A.; Schlegel, H. B.; Fluder, E. M.; Pople, J. A. *GAUSSIAN 82*; Carnegie-Mellon University: Pittsburgh, 1983.
(50) Pople, J. A.; Nesbet, R. K. *J. Chem. Phys.* **1954**, *27*, 571.
(51) Schlegel, H. B. *J. Comput. Chem.* **1982**, *3*, 214.
(52) Binkley, J. S.; Pople, J. A.; Hehre, W. J. *J. Am. Chem. Soc.* **1980**, *102*, 939.

culated with fourth order Møller–Plesset perturbation theory[54] in the space of single, double, and quadruple excitations (MP4SDQ, frozen core) with the 6-31G** basis (d type polarization functions on heavy atoms and p type on hydrogen) at the HF/6-31G* optimized geometry. Vibrational frequencies and zero-point energies were obtained from analytical second derivatives[55] calculated at the HF/3-21G level.

The effect of spin contamination was examined by annihilation of the largest spin contaminant in the UHF wave function.[56,57] The annihilation operator that removes the s + 1 spin component can be written as

$$\hat{A}_{s+1} = \frac{\hat{S}^2 - (s+1)(s+2)}{\langle\Psi_0|\hat{S}^2|\Psi_0\rangle - (s+1)(s+2)} \tag{1}$$

After annihilation of the s + 1 component, the approximate projected Hartree–Fock energy and wave function are

$$\begin{aligned} E_{\mathrm{PUHF}} &= \frac{\langle\Psi_0|\hat{H}|\hat{A}_{s+1}\Psi_0\rangle}{\langle\Psi_0|\hat{A}_{s+1}\Psi_0\rangle} \\ &= \langle\Psi_0|\hat{H}|\Psi_0\rangle + \frac{\sum_{i\neq 0}\langle\Psi_0|\hat{H}|\psi_i\rangle\langle\psi_i|\hat{A}_{s+1}|\Psi_0\rangle}{\langle\Psi_0|\hat{A}_{s+1}|\Psi_0\rangle} \\ &= E_{\mathrm{UHF}} + \Delta E_{\mathrm{PUHF}} \end{aligned} \tag{2}$$

$$\hat{A}_{s+1}\Psi_0 = \Psi_0 + \tilde{\Psi}_1 = \Psi_0 + \frac{\sum_{j\neq 0}\psi_j\langle\psi_j|\hat{A}_{s+1}|\Psi_0\rangle}{\langle\Psi_0|\hat{A}_{s+1}|\Psi_0\rangle} \tag{3}$$

For $\tilde{\Psi}_1$, ψ_j runs over all single excitations and all $\alpha\beta$ type double excitations. Perturbative corrections for electron correlation, Ψ_1, Ψ_2, etc., also consist of single, double, and higher excitations. As a first approximation to spin-projected UMP*n* energies, the spin correction $\tilde{\Psi}_1$ must be reduced by the amount already contained in Ψ_1, Ψ_2, etc. This leads to the following approximate formulas

$$E_{\mathrm{PMP2}} = E_{\mathrm{UMP2}} + \Delta E_{\mathrm{PUHF}}\left\{1 - \frac{\langle\tilde{\Psi}_1|\Psi_1\rangle}{\langle\tilde{\Psi}_1|\tilde{\Psi}_1\rangle}\right\} \tag{4}$$

$$E_{\mathrm{PMP3}} = E_{\mathrm{UMP3}} + \Delta E_{\mathrm{PUHF}}\left\{1 - \frac{\langle\tilde{\Psi}_1|\Psi_1 + \Psi_2\rangle}{\langle\tilde{\Psi}_1|\tilde{\Psi}_1\rangle}\right\} \tag{5}$$

$$\begin{aligned} E_{\mathrm{PMP4}} &= E_{\mathrm{UMP4}} + \Delta E_{\mathrm{PUHF}}\left\{1 - \frac{\langle\tilde{\Psi}_1|\Psi_1 + \Psi_2 + \Psi_3\rangle}{\langle\tilde{\Psi}_1|\tilde{\Psi}_1\rangle}\right\} \\ &\approx E_{\mathrm{UMP4}} + \Delta E_{\mathrm{PUHF}}\left\{1 - \frac{\langle\tilde{\Psi}_1|\Psi_1 + \Psi_2\rangle}{\langle\tilde{\Psi}_1|\tilde{\Psi}_1\rangle}\right\} \end{aligned} \tag{6}$$

These approximations have been used successfully in our previous studies.[37,42,56] The total energies at the highest level were estimated by adding the correction for spin contamination (PMP4/6-31G* − MP4/6-31G*) and for zero-point energies (ZPE/3-21G) to the MP4/6-31G** energies.

Results and Discussion

The optimized equilibrium geometries and transition structures are collected in Figures 1–4. The corresponding total energies are in Table I. In general there is good agreement between the HF/3-21G and the HF/6-31G* values. Angles change by less than ±1°, bond lengths by ±0.005 Å, with slightly larger variations for the parameters involving attacking or migrating groups. Exceptions include the pyramidal angles at carbon-centered radicals (*slightly* more pyramidal at HF/6-31G*), torsional angles of nearly free rotors, and bonds involving oxygen (ΔR_{CO} = +0.04 Å, ΔR_{OH} = −0.02 Å). Calculations on F + C_2H_4[40,41] and on two heavy-atom systems[58] indicate that the inclusion of correlation

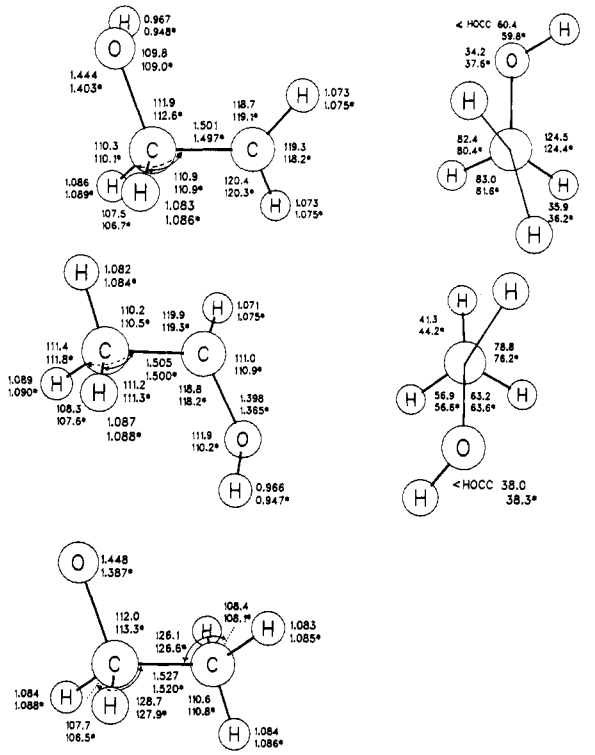

Figure 1. Geometries of 2-hydroxyethyl, 1-hydroxyethyl, and ethoxy radicals: HF/3-21G optimized (no superscript), HF/6-31G* optimized (asterisk), in Å and deg (bond lengths and valence angles on the left, dihedral angles on the right).

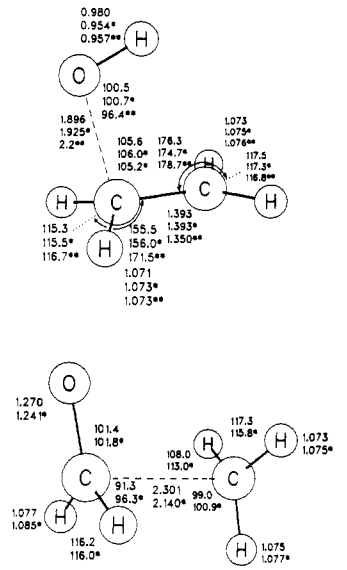

Figure 2. Geometries of the OH + C_2H_4 and CH_3 + CH_2O transition states: HF/3-21G optimized (no superscript), HF/6-31G* optimized (asterisk), in Å and deg. For OH + C_2H_4, several additional points along the reaction path were obtained by fixing R(C–O) and optimizing all of the remaining parameters at HF/6-31G*. At the PMP4/6-31G* level, the barrier along this reaction path occurs near R(C–O) = 2.2 Å (double asterisk).

(53) Hehre, W. J.; Ditchfield, R.; Pople, J. A. *J. Chem. Phys.* **1972**, *56*, 2257. Hariharan, P. C.; Pople, J. A. *Chem. Phys. Lett.* **1972**, *66*, 217.
(54) Møller, C.; Plesset, M. S. *Phys. Rev.* **1934**, *46*, 618. (b) Bartlett, R. J. *Annu. Rev. Phys. Chem.* **1981**, *32*, 359.
(55) Pople, J. A.; Krishnan, R.; Schlegel, H. B.; Binkley, J. S. *Int. J. Quantum Chem., Quantum Chem. Symp.* **1979**, *13*, 225.
(56) Schlegel, H. B. *J. Chem. Phys.* **1986**, *84*, 4530.
(57) For a review of spin projection methods see: Mayer, I. *Adv. Quantum Chem.* **1980**, *12*, 189.
(58) DeFrees, D. J.; Raghavachari, K.; Schlegel, H. B.; Pople, J. A. *J. Am. Chem. Soc.* **1982**, *104*, 5576.

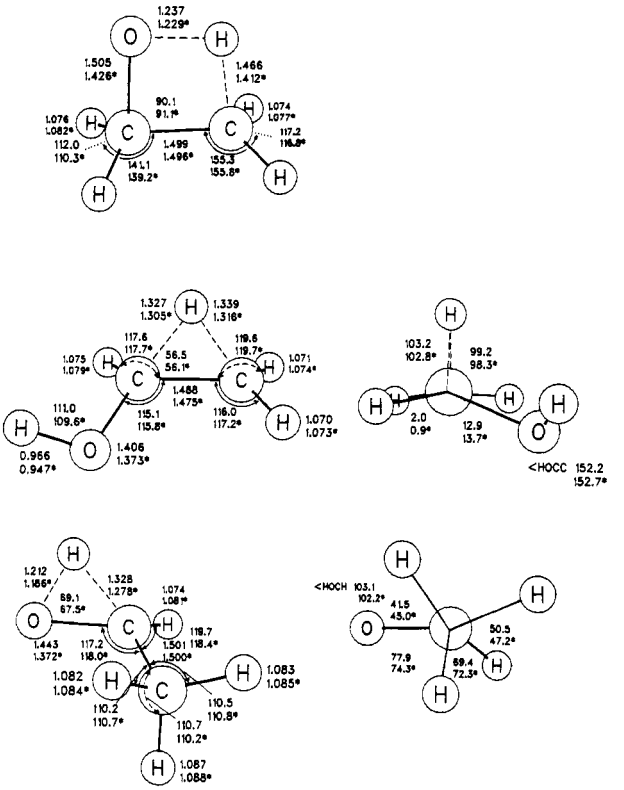

Figure 3. Transition structures for hydrogen sigmatropic shifts: HF/3-21G optimized (no superscript), HF/6-31G* optimized (asterisk), in Å and deg (bond lengths and valence angles on the left, dihedral angles on the right).

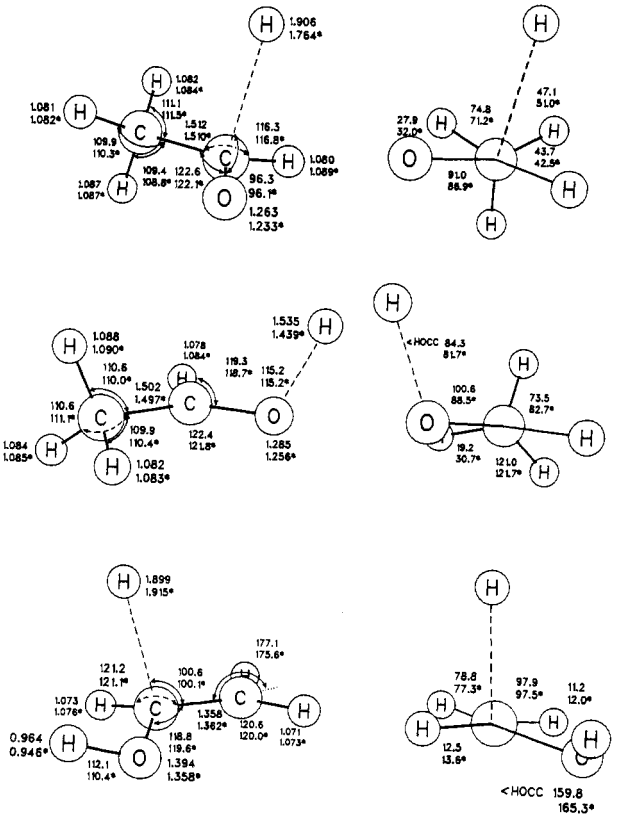

Figure 4. Transition structures for hydrogen addition: HF/3-21G optimized (no superscript), HF/6-31G* optimized (asterisk), in Å and deg (bond lengths and valence angles on the left, dihedral angles on the right).

energy causes only small systematic changes in the optimized geometry, the largest being C—O and C=C (ΔR = +0.01 Å), C=O and O—H (ΔR = 0.02 Å); angles remain relatively

Table I. Total Energies

molecule	HF/3-21G	HF/6-31G*	MP2/6-31G*	MP3/6-31G*	MP4/6-31G*	PMP4/6-31G*	HF/6-31G**	MP2/6-31G**	MP3/6-31G**	MP4/6-31G**	ZPE/3-21G
minima											
$OH + C_2H_4$	−152.571 22	−153.414 00	−153.804 99	−153.837 90	−153.845 09	−153.845 89	−153.427 16	−153.848 74	−153.883 96	−153.890 01	39.8
$CH_3 + CH_2O$	−152.564 43	−153.425 33	−153.833 92	−153.856 21	−153.867 08	−153.868 27	−153.434 20	−153.873 90	−153.898 96	−153.909 04	37.6
$CH_3CHO + H$	−152.551 45	−153.414 20	−153.842 77	−153.858 56	−153.868 40	−153.868 40	−153.420 81	−153.874 57	−153.892 42	−153.901 34	37.5
$HOCHCH_2 + H$	−152.537 96	−153.387 11	−153.816 52	−153.835 16	−153.842 59	−153.842 59	−153.399 20	−153.852 60	−153.872 97	−153.879 40	38.1
$HOCH_2CH_2$	−152.591 65	−153.443 28	−153.855 68	−153.881 19	−153.888 45	−153.889 64	−153.456 48	−153.899 89	−153.927 77	−153.933 91	43.3
$HOCHCH_3$	−152.600 25	−153.451 32	−153.867 82	−153.892 17	−153.899 99	−153.900 98	−153.464 57	−153.912 05	−153.938 73	−153.945 34	43.9
OCH_2CH_3	−152.616 40	−153.460 94	−153.856 13	−153.887 72	−153.895 23	−153.895 95	−153.468 88	−153.896 28	−153.930 55	−153.936 72	43.9
transition structures											
$OCH_2CH_3 \rightarrow CH_2O + CH_3$	−152.561 82	−153.411 89	−153.811 07	−153.838 53	−153.850 17	−153.861 20	−153.419 72	−153.851 27	−153.881 45	−153.892 05	40.3
$HOCH_2CH_2 \rightarrow OCH_2CH_3$	−152.528 95	−153.370 48	−153.797 47	−153.821 53	−153.831 17	−153.836 08	−153.382 40	−153.841 05	−153.867 20	−153.875 60	40.9
$HOCH_2CH_2 \rightarrow HOCHCH_3$	−152.494 44	−153.352 11	−153.780 30	−153.803 46	−153.811 57	−153.815 17	−153.368 35	−153.826 82	−153.851 84	−153.858 72	40.1
$HOCHCH_3 \rightarrow OCH_2CH_3$	−152.520 59	−153.374 25	−153.801 09	−153.824 23	−153.833 62	−153.837 47	−153.386 92	−153.844 90	−153.870 09	−153.878 22	40.4
$OCH_2CH_3 \rightarrow CH_3CHO + H$	−152.544 11	−153.399 22	−153.811 70	−153.834 52	−153.845 64	−153.855 47	−153.406 20	−153.845 87	−153.870 83	−153.880 84	38.2
$HOCHCH_3 \rightarrow CH_3CHO + H$	−152.536 58	−153.385 15	−153.800 87	−153.823 94	−153.835 37	−153.846 65	−153.383 04	−153.836 75	−153.861 90	−153.872 30	37.9
$HOCH_2CH_2 \rightarrow HOCHCH_2 + H$	−152.525 02	−153.374 61	−153.789 55	−153.811 86	−153.821 01	−153.831 41	−153.387 12	−153.827 84	−153.851 93	−153.860 13	38.0

[a] Total energies in au, zero-point energies in kcal/mol.

Table II. Vibrational Frequencies[a]

molecule	frequencies (cm^{-1})
minima	
OH	3609 (3735)
CH_3	424 (580), 1544 (1383), 1544 (1383), 3251 (3002), 3251 (3002), 3428 (3184)
CH_2O	1337 (1167), 1378 (1249), 1692 (1500), 1916 (1746), 3162 (2783), 3233 (2843)
C_2H_4	944 (826), 1115 (949), 1157 (943), 1165 (1023), 1387 (1236), 1522 (1242), 1640 (1444), 1842 (1623), 3238 (3026), 3305 (2989), 3371 (3103), 3403 (3106)
CH_3CHO	162 (150), 531 (509), 889 (764), 939 (867), 1222 (1114), 1271 (1102), 1555 (1352), 1565 (1395), 1628 (1433), 1645 (1448), 1926 (1743), 3159 (2716), 3200 (2923), 3248 (2968), 3307 (3614)
$HOCHCH_2$	463 (413), 529, 779 (819), 1036 (1084), 1041, 1156, 1184, 1453, 1478, 1612, 1849 (1631), 3331, 3396, 3427, 3889, (3625)
$HOCH_2CH_2$	215, 372, 435, 525, 908, 993, 1117, 1195, 1293, 1488, 1525, 1576, 1675, 3182, 3219, 3300, 3412, 3862
$HOCHCH_3$	197, 321, 415, 670, 937, 1130, 1147, 1230, 1410, 1510, 1574, 1652, 1662, 3158, 3207, 3269, 3360, 3879
OCH_2CH_3	154, 352, 421 (442), 908 (873), 1000, 1071 (1067), 1203, 1397, 1504 (1342), 1577, 1631, 1659, 1670, 3201, 3210, 3230, 3270, 3281
transition structures	
OH + C_2H_4 → $HOCH_2CH_2$	556i, 97, 304, 474, 820, 895, 982, 1042, 1091, 1271, 1361, 1620, 1673, 3303, 3337, 3388, 3426, 3690
OCH_2CH_3 → CH_2O + CH_3	321i, 94, 242, 515, 563, 679, 893, 1082, 1326, 1335, 1564, 1572, 1707, 3226, 3250, 3317, 3404, 3417
$HOCH_2CH_2$ → OCH_2CH_3	2599i, 412, 713, 876, 899, 1047, 1107, 1128, 1205, 1340, 1394, 1579, 1683, 1913, 3281, 3307, 3343, 3410
$HOCHCH_3$ → OCH_2CH_3	2513i, 170, 418, 674, 923, 970, 1144, 1186, 1212, 1474, 1574, 1647, 1660, 2147, 3185, 3246, 3278, 3332
$HOCH_2CH_2$ → $HOCHCH_3$	2546i, 355, 394, 449, 872, 899, 1006, 1154, 1229, 1354, 1383, 1515, 1548, 1939, 3303, 3327, 3452, 3869
OCH_2CH_3 → CH_3CHO + H	805i, 183, 455, 493, 524, 922, 959, 1180, 1210, 1391, 1561, 1569, 1649, 1654, 3195, 3236, 3262, 3303
$HOCHCH_3$ → CH_3CHO + H	1293i, 110, 331, 511, 664, 826, 939, 1162, 1207, 1349, 1554, 1566, 1646, 1651, 3177, 3241, 3269, 3294
$HOCH_2CH_2$ → $HOCHCH_2$ + H	828i, 274, 466, 504, 541, 679, 890, 998, 1073, 1211, 1309, 1398, 1576, 1669, 3333, 3344, 3438, 3900

[a] Experimental frequencies in parentheses.

unaffected. Except for some transition states, such as OH + C_2H_4,[37] the effects of spin projection on geometry would appear to be small.[59]

The vibrational frequencies are collected in Table II. On average the HF/3-21G frequencies for molecules containing first-row atoms are ca. 11% too high when compared to the experimental anharmonic frequencies (more than 500 comparisons) due to a combination of basis set effects, electron correlation, and vibrational anharmonicity.[60] The transition vectors are shown in Figure 5.

(59) Based on studies of the effects of spin projection and electron correlation on barrier heights and positions in the following reactions: OH + C_2H_2,[37] OH + C_2H_4[37] (reaction I), CH_3 + C_2H_4,[64] CH_3 + CH_2O[64] (reaction III), H + C_2H_2[70] (suitable as a model for reactions IV, VII and VIII), CH_3O → CH_2OH,[69] CH_3 + H_2,[69] and CH_3 + H_2O[69] (models for reactions II, V, and VI).

(60) Pople, J. A.; Schlegel, H. B.; Krishnan, R.; DeFrees, D. J.; Binkley, J. S.; Frisch, M. J.; Whiteside, R. A.; Hout, R. F.; Hehre, W. J. *Int. J. Quantum Chem., Quantum Chem. Symp.* **1981**, *15*, 269.

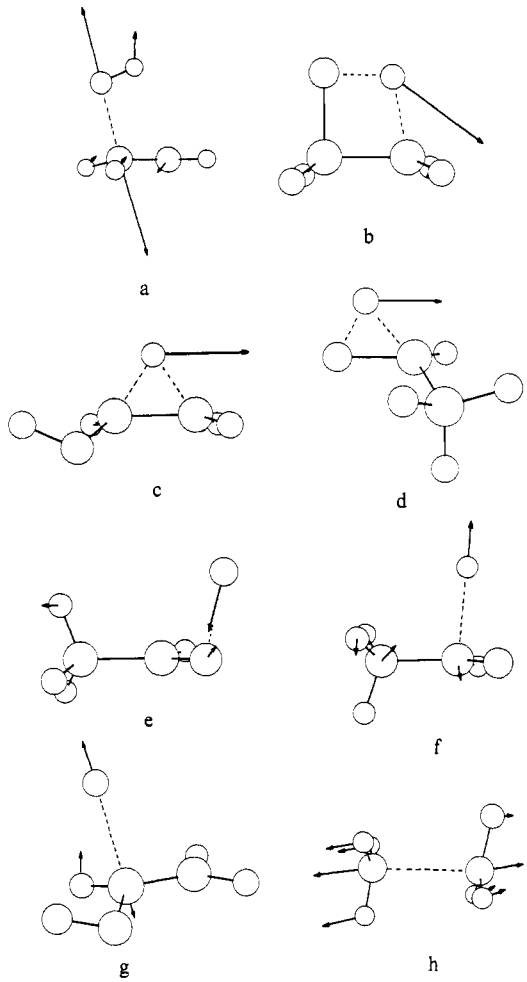

Figure 5. Transition vectors for (a) OH + C_2H_4 → $HOCH_2CH_2$, (b) $HOCH_2CH_2$ → CH_3CH_2O, (c) $HOCH_2CH_2$ → $HOCHCH_3$, (d) $HOCHCH_3$ → CH_3CH_2O, (e) CH_3CHO + H → $HOCHCH_3$, (f) CH_3CH_2O → CH_3CHO + H, (g) $HOCH_2CH_2$ → $HOCHCH_2$ + H and (h) CH_3CH_2O → CH_3 + CH_2O.

Relative energies, isodesmic reaction energies, and barrier heights are listed in Tables III–V. The treatment of the energetics is somewhat involved due to sizable basis set effects, correlation effects, and spin contamination. Therefore the heats of reaction and barrier heights are analyzed in separate sections following the discussion of the geometries and frequencies of the individual intermediates and transition structures.

OH + C_2H_4 → $HOCH_2CH_2$. Details of this addition reaction have been discussed in a previous paper;[37] the geometry of the transition state is shown in Figure 2a. Prior to the transition state, OH forms a hydrogen-bonded complex with the ethylene π orbital, analogous to the HF + C_2H_4 complex.[61] At the HF and MP*n* levels the barrier height for OH addition is overestimated by 7–10 kcal/mol. After spin annihilation the barrier is reduced to −0.9 kcal/mol and shifted 0.3 Å closer to the reactants. The barrier height corresponds to a calculated activation energy of 0.1 kcal/mol which is in good agreement with the experimental activation energy (−0.9 ± 0.3 kcal/mol).[2,14,17,19] Because the barrier height is so small, the barrier position is quite sensitive to spin annihilation. For other reactions with larger barriers, spin projection displaces the transition structures by less than 0.1 Å;[59] such displacements change the barrier heights by less than 1 kcal/mol for the reactions studied.[59]

$HOCH_2CH_2$. Several experimental and theoretical studies on the conformational preferences of β-substituted ethyl radicals[25,26,47] indicate that the barrier to the CC bond rotation is quite low. Pross and Radom[47] found the eclipsed conformation **1b** to be 0.7

(61) Shea, J. A.; Flygare, W. H. *J. Chem. Phys.* **1982**, *76*, 4857.

Table III. Energies Relative to OH + C_2H_4[a]

level	$HOCH_2CH_2$	$HOCHCH_3$	OCH_2CH_3	$CH_3 + CH_2O$	$CH_3CHO + H$	$HOCHCH_2 + H$
HF/3-21G	−12.8	−18.2	−28.4	4.3	12.4	20.9
HF/6-31G*	−18.4	−23.4	−29.2	−7.1	−0.1	16.9
MP2/6-31G*	−31.8	−39.4	−31.9	−18.2	−23.7	−7.2
MP3/6-31G*	−27.2	−34.1	−31.0	−11.5	−13.0	1.7
MP4SDQ/6-31G*	−27.2	−34.5	−31.2	−13.8	−14.6	1.6
PMP4/6-31G*	−27.5	−34.6	−31.4	−14.0	−14.1	2.1
HF/6-31G**	−18.4	−23.5	−26.2	−4.4	−0.5	17.5
MP2/6-31G**	−32.1	−39.7	−29.8	−15.8	−16.2	−2.4
MP3/6-31G**	−27.5	−34.4	−29.2	−9.4	−5.3	6.9
MP4SDQ/6-31G**	−27.6	−34.7	−29.3	−12.0	−7.1	6.7
ZPE/3-21G	3.5	4.2	4.2	−2.1	−2.2	−1.7
theoretical $\Delta H°$(0 K)	−24.4	−30.6	−25.3	−14.3	−8.8	5.5
experimental $\Delta H°$(0 K)	−28.9	−34.4	−25.9	−13.6	−9.5	0.4

[a] Energy in kcal/mol.

Table IV. Isodesmic Reaction Energies[a]

level	$C_2H_4 + CH_3OH \rightarrow CH_4 + HOCHCH_2$	$C_2H_5 + HOCHCH_2 \rightarrow C_2H_4 + HOCH_2CH_2$	$C_2H_5 + CH_3OH \rightarrow CH_4 + HOCH_2CH_2$	$HOCH_2CH_2 \rightarrow HOCHCH_3$
HF/3-21G	−9.3	−4.3	5.0	−5.4
HF/6-31G*	−10.6	−3.7	4.2	−5.0
MP2/6-31G*	−13.5	−4.9	8.6	−7.6
MP3/6-31G*	−12.1	−4.6	7.5	−6.9
MP4SDQ/6-31G*	−12.3	−4.7	7.6	7.2
PMP4/6-31G*	−12.3	−5.2	7.1	−7.1
HF/6-31G**	−10.8	−3.9	7.0	−5.1
MP2/6-31G**	−13.1	−4.7	8.4	−7.6
MP3/6-31G**	−11.6	−4.3	7.3	−6.9
MP4SDQ/6-31G**	−11.8	−4.6	7.2	−7.2
ZPE/3-21G	−1.4	−1.3	0.1	0.6
theor $\Delta H°$(0 K)	−13.2	−6.4	6.8	−6.5
exptl $\Delta H°$(0 K)	−12.3	−6.3	6.0	−5.5

[a] Energy in kcal/mol.

Table V. Barrier Heights[a]

level	$OCH_2CH_3 \rightarrow CH_3 + CH_2O$	$HOCH_2CH_2 \rightarrow CH_3CH_2O$	$HOCH_2CH_2 \rightarrow HOCHCH_3$	$HOCHCH_3 \rightarrow CH_3CH_2O$	$H + HOCHCH_2 \rightarrow HOCH_2CH_2$	$H + CH_3CHO \rightarrow OCH_2CH_3$	$H + CH_3CHO \rightarrow HOCHCH_3$
HF/3-21G	34.2	39.3	61.0	50.0	8.1	4.6	9.5
HF/6-31G*	30.8	45.7	57.2	48.4	7.7	9.4	18.2
MP2/6-31G*	28.3	36.5	47.3	41.9	16.9	19.5	26.3
MP3/6-31G*	30.9	37.4	48.8	42.6	14.6	15.1	21.7
MP4SDQ/6-31G*	28.3	35.9	48.2	41.7	13.5	14.3	20.7
PMP4/6-31G*	22.1	33.6	46.7	39.9	7.0	8.1	13.6
HF/6-31G**	30.8	46.5	55.3	48.7	7.6	9.2	17.4
MP2/6-31G**	28.2	36.9	45.8	42.1	15.6	13.6	19.1
MP3/6-31G**	30.8	38.0	47.7	43.1	13.2	13.6	19.1
MP4SDQ/6-31G**	28.0	36.6	47.2	42.1	12.1	12.9	18.2
ZPE/3-21G	−3.6	−2.4	−3.2	−3.6	−0.1	0.7	0.4
theoretical $\Delta H°$(0 K)	18.2	31.9	42.5	36.7	5.5	5.9	10.8
experimental $\Delta H°$(0 K)	20–22						

[a] Energy in kcal/mol.

Chart I

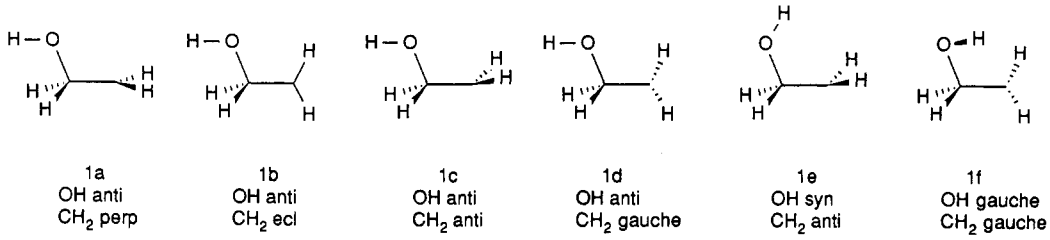

kcal/mol lower than the perpendicular form **1a** at the HF/3-21G level using standard geometries and assuming a planar radical center. When the OH is constrained to be anti, the present calculations with geometry optimization at the HF/6-31G* level support the earlier results. The radical center is slightly pyramidal, but it is a single well potential rather than a double well (i.e., no inversion). In ethyl radical, correlation corrections favor a more planar geometry.[62] The CH_2 anti conformation **1c**, corresponding

(62) Davidson, E. R. *Theor. Chim. Acta* **1985**, *68*, 57.
(63) Schlegel, H. B.; Sosa, C. *J. Phys. Chem.* **1984**, *88*, 1141.
(64) Gonzalez, G.; Sosa, C.; Schlegel, H. B., to be published.

to **1a**, is a transition structure for methylene rotation (57i cm^{-1}); the gauche conformation **1d** is 0.5 kcal/mol lower at HF/6-31G*. Other conformations of the OH must also be considered. The syn addition of OH to C_2H_4 leads to conformation **1e**. However, **1e** is a transition structure with respect to OH rotation (312i cm^{-1}). The global minimum for $HOCH_2CH_2$ is the OH gauche, CH_2 gauche structure **1f** shown in Figure 1. Relative to **1f**, the energies of **1c**, **1d**, and **1e** are 1.4, 1.0, and 2.1 kcal/mol, respectively, at the HF/6-31G* level.

The ESR spectrum of $HOCH_2CH_2$ has been observed as a minor component in the photolysis of ethanol,[27] and also directly in the reduction of $HOCH_2CH_2I$.[24] The splitting pattern is only approximately that expected for a compound with two equivalent pairs of protons. Some additional splitting was observed and ascribed to the non-equivalence of the α and/or the β protons. This is in agreement with the present calculations that yield a nonsymmetric gauche, gauche structure **1f** as the minimum.

The infrared spectrum of $HOCH_2CH_2$ has not been observed. However, like FCH_2CH_2,[40] there is a low-frequency CH stretch calculated for the gauche conformer. This corresponds to the β CH that is anti to the half-filled p orbital of the radical center (3182 cm^{-1} calculated for OH versus 3192 calculated and 2852 observed for F). These calculations suggest that the experimental spectrum of $HOCH_2CH_2$ should also contain a CH stretch near 2850 cm^{-1} that is diagnostic of C–H bonds β to a radical center.

$HOCH_2CH_2$ → OCH_2CH_3. One of the lower energy paths proposed for the unimolecular decomposition of $HOCH_2CH_2$ is a [1,3] shift of hydrogen to form OCH_2CH_3.[16,19] The optimized geometry for the transition structure shown in Figure 3a is a tight four-membered ring midway along the path between $HOCH_2CH_2$ and OCH_2CH_3. The OH and CH distances are both ca. 30% longer than their regular covalent values, and the OCC angle has been compressed from 113° to 91°. The transition vector, Figure 5b, is almost exclusively H migration and corresponds to a large imaginary frequency (2599i cm^{-1}), suggesting that tunneling could be important. The $HOCH_2CH_2$ → OCH_2CH_3 reaction can also be considered an internal radical abstraction. Calculations on CH_4 + OH → CH_3 + H_2O[69] indicate that spin projection and electron correlation do not change the position of the transition state significantly.

$HOCH_2CH_2$ → $HOCHCH_3$. The geometry of the [1,2]-shift transition state, Figure 3b, is very similar to CH_3CH_2 → CH_2CH_3 computed at an equivalent level.[46] In both cases the migrating hydrogen is ca. 1.08 Å above the midpoint of the CC bond. Other orientations of the OH group in the transition structure are possible, but they are probably similar in energy. The effect of spin projection on the geometry of the transition state is expected to be small. In a study of a related [1,2] shift, the position of the transition state for CH_3O → CH_2OH was not altered significantly by spin projection or electron correlation. The [1,2] shift in $HOCH_2CH_2$ is 10–12 kcal/mol higher than the [1,3] shift. This difference could be attributed to the difference in strain between the three-membered ring and the four-membered rings, but this is not supported by the optimized geometry of the transition state. Greater strain would suggest bond elongation to partially relieve the strain. By contrast, the C–H distances in the transition structure are only ca. 22% elongated compared to ca. 30% in the [1,3]-shift transition state. Similarly the CC bond is shorter and the $HOCHCH_2$ moiety is flatter than in either $HOCH_2CH_2$ or $HOCHCH_3$, looking more like vinyl alcohol.

$HOCH_2CH_2$ → $HOCHCH_2$ + H. The structure of the hydrogen plus vinyl alcohol transition state is very similar to that of H + C_2H_4,[42,46] H + C_2H_3F,[40,41] H + C_2H_3Cl,[63] and H + C_2H_2.[70] In all these cases, the hydrogen is ca. 1.9 Å from the carbon and makes an angle of ca. 105° with the C=C bond. The $HOCHCH_2$ is nearly planar and the C=C bond is only slightly elongated. Viewed as an addition, the transition state can be described as early but tight. The transition structure occurs earlier along the reaction path than H + C_2H_3F, but later than H + C_2H_4 and H + C_2H_3Cl. In H + C_2H_2,[70] the PMP4/6-31G* optimized geometry was found to be very similar to the UHF/6-31G* geometry.

$HOCHCH_2$. In agreement with the microwave spectrum[30] and with previous theoretical calculations,[38,39] the syn structure of vinyl alcohol is found to be more stable. The calculated frequencies support the assignment of the experimental infrared spectrum.[31] In particular the OH torsion mode is found at an unusually high frequency (463 cm^{-1} calculated, 413 cm^{-1} observed).

$HOCHCH_3$. The optimized geometry of 1-hydroxyethyl radical is presented in Figure 1b. Because of the electronegative substituent at the radical center, 1-hydroxyethyl radical is somewhat more pyramidal than 2-hydroxyethyl radical. Cirelli, Ha, Meyer, and Gunthard[23] have calculated the internal rotation inversion surface for 1-hydroxyethyl radical and used this surface to interpret the temperature dependence of the ESR spectrum.[23,27]

OCH_2CH_3. Like CH_3O, ethoxy radical has a $^2A'$ ground state. Compared to the 1- and 2-hydroxyethyl radicals, the C–O bond length in ethoxy appears to be more sensitive to polarization functions. Portions of the vibrational spectrum of ethoxy radical have been observed by laser-induced fluorescence of radicals produced by the reaction of ethanol and fluorine atoms.[27] The calculated mode at 1071 cm^{-1} is dominated by CO stretch and may correspond to the observed 1067 cm^{-1} band. Other ground-state modes deduced from the spectra include ~442 cm^{-1} (421 calculated, CCO bend), ~873 cm^{-1} (908, CC stretch), and ~1342 cm^{-1} (1504, CH_2 wag).

OCH_2CH_3 → CH_2O + CH_3. The lowest energy path for the unimolecular reaction of ethoxy radical is decomposition into formaldehyde and methyl radical. The calculated transition structure is shown in Figure 2b. Although the CH_3 + CH_2O addition barrier is relatively small and spin contamination is fairly large, the position of the transition state is not shifted significantly by spin projection.[64] The CH_3 is ca. 2.4 Å from the CH_2O, similar to the transition state found for CH_3 + C_2H_4,[64,65] but somewhat longer than other first-row radicals adding to C_2H_4. Both the CH_2O and the CH_3 groups are slightly pyramidal. For the family of X + CH_2O addition reactions, the transition state for X = CH_3 occurs earlier along the reaction path than that for X = H, as gauged by the C=O bond length and the CH_2O pyramidality. The transition state has a low-frequency CH_3 torsion mode (94 cm^{-1}) as well as one imaginary frequency mode (321i cm^{-1}, C–C stretch).

OCH_2CH_3 → CH_3CHO + H. A second, higher energy pathway for the decomposition of ethoxy radical is the loss of hydrogen to form acetaldehyde. This pathway is not observed experimentally for OCH_2CH_3, but it may be compared to CH_3O → CH_2O + H.[42–45] Like the latter, the transition state occurs at a C–H distance of ca. 1.8 Å. The C–CHO group is only slightly pyramidal, and the hydrogen makes an angle of 96° to the C=O bond. By comparison with H + C_2H_2,[70] the effect of spin projection on the transition-state geometry is expected to be small.

OCH_2CH_3 → $HOCHCH_3$. Aside from decomposition, ethoxy radical can undergo [1,2]- and [1,3]-hydrogen shifts. The [1,3] shift forming CH_3CHOH was discussed above. A [1,2] shift leads to 1-hydroxyethyl radical. The transtion state is very similar in terms of energy, structure, and vibrational frequencies to CH_3O → CH_2OH, recently studied by Saebø, Radom, and Schaefer,[43] Adams, Bartlett, and Purvis,[44] and Harding.[45] The position of the transition state for CH_3O → CH_2OH does not change significantly when re-optimized with spin projection and electron correlation.[69]

Heats of Reaction and Relative Energies. Reliable heats of formation are available for most of the closed-shell species and

(65) Canadell, E.; Poblet, J. M.; Olivella, S. *J. Phys. Chem.* **1983**, *87*, 424.
(66) Stull, D. R.; Prophet, H. *JANAF Thermochemical Tables*; U.S. Government Printing Offices: Washington, DC, 1971, and subsequent supplements.
(67) Castelhano, A. T.; Marriot, P. R.; Griller, R. *J. Am. Chem. Soc.* **1981**, *103*, 4262.
(68) Frisch, M. J.; Binkley, J. S.; Schaefer, H. F., III *J. Chem. Phys.* **1984**, *81*, 1882.
(69) Schlegel, H. B., unpublished calculations at the PMP4/3-21G level.
(70) Schlegel, H. B.; Sosa, C. *Int. J. Quantum Chem., Quantum Chem. Symp.*, in press.

some of the radicals ($\Delta H_f°(0\ K)$ = 14.6, −25.0, −36.9, 51.6, 9.3, 35.6, and −0.3 kcal/mol for C_2H_4, CH_2O, CH_3CHO, H, OH, CH_3, and CH_3CH_2O, respectively).[29,32,35,66] The heat of formation of vinyl alcohol is somewhat less certain[36] ($\Delta H_f°(0\ K)$ = −27 ± 2 kcal/mol). The C–H bond strength in C_2H_6 (D_0 = 100.7 ± 1 kcal/mol at 300 K, 98.5 kcal/mol at 0 K)[67] can be combined with the $\Delta H_f°(0\ K)$ = −51.5 kcal/mol for ethanol to yield an estimated $\Delta H_f°(0\ K)$ = −5.0 kcal/mol for $HOCH_2CH_2$; similarly, the C–H bond strength in CH_3OH (D_0 = 93 kcal/mol)[35] and $\Delta H_f°(0\ K)$ of ethanol provide an estimated $\Delta H_f°(0\ K)$ = −10.5 kcal/mol for $HOCHCH_3$.

Table III lists the calculated heats of reaction for the OH + C_2H_4 system. For the products $CH_2O + CH_3$, CH_3CHO + H, and OCH_2CH_3, the agreement is quite good, despite sizable basis set and correlation effects. The good agreement can probably be attributed to a fortuitous cancellation of errors, since some of the other heats of reaction are not predicted as well.

At the highest level of calculation, the ΔH for OH + $C_2H_4 \rightarrow HOCHCH_2$ + H is overestimated by ca. 5 kcal/mol. Similar calculations were carried out for OH + $CH_4 \rightarrow CH_3OH$ + H, which also involves the breaking of a CH bond and the formation of a CO bond, but for which all the heats of formation are well-known. This reaction is also overestimated by 5 kcal/mol at the same level of calculation. The difference between these two reactions is an isodesmic reaction

$$C_2H_4 + CH_3OH \rightarrow HOCHCH_2 + CH_4 \qquad (7)$$

The calculated heat of reaction for eq 7 is much less sensitive to the computational level and agrees well with experiment, as can be seen in Table IV.

The energy of CH_3CH_2O relative to OH + C_2H_4 is in good agreement with experiment, whereas the relative energy of $HOCH_2CH_2$ and $HOCHCH_3$ appear to be too high by ca. 4 kcal/mol (Table III). This may be a reflection of the fact that CH_3CH_2O and the reactants are both oxygen radicals, while $HOCH_2CH_2$ and $HOCHCH_3$ are carbon-centered radicals. On the other hand, the experimental estimated heat of formation used for $HOCH_2CH_2$ and $HOCHCH_3$ may be in error, or the level of theory may be inadequate. The following two isodesmic reactions are relatively insensitive to basis set and correlation problems (see Table IV)

$$C_2H_5 + CH_3OH \rightarrow HOCH_2CH_2 + CH_4 \qquad (8)$$

$$C_2H_5 + CH_3OH \rightarrow HOCHCH_3 + CH_4 \qquad (9)$$

and can be used to calculate a better theoretical estimate of the $\Delta H_f°$ for the radicals, given the experimental $\Delta H_f°$'s of C_2H_5, CH_3OH, and CH_4. These reactions yield $\Delta H_f°$ = −5.1 kcal/mol for $HOCH_2CH_2$ and −11.6 for $HOCHCH_3$, in very good agreement with the experimental estimates (−5.0 and −10.5 kcal/mol, respectively). Alternatively, the experimental heat of formation of vinyl alcohol[36] can be used in

$$HOCHCH_2 + C_2H_5 \rightarrow C_2H_4 + HOCH_2CH_2 \qquad (10)$$

$$HOCHCH_2 + C_2H_5 \rightarrow C_2H_4 + HOCHCH_3 \qquad (11)$$

resulting in $\Delta H_f°$ = −4.2 and −10.7 kcal/mol for $HOCH_2CH_2$ and $HOCHCH_3$, also in very good agreement with experiment. Similar agreement can be found by using $CH_3CH_2OH + CH_3CH_2 \rightarrow C_2H_6 + HOCH_2CH_2$.

Barrier Heights. Experimental activation energies are available for only two of the reactions in Scheme I. The activation energy for OH + C_2H_4 is −0.9 ± 0.3 kcal/mol.[2,14,17,19] Thermal decomposition of ethoxy radical[32–34] gives an activation energy of 20–22 kcal/mol for $CH_3CH_2O \rightarrow CH_2O + CH_3$ and indicates that other processes such as $CH_3CH_2O \rightarrow CH_3CHO$ + H and $CH_3CH_2O \rightarrow HOCHCH_3$ have higher barriers.

The calculated barrier for OH + C_2H_4 is 7–10 kcal/mol too high at the HF and MP*n* levels due to spin contamination in the transition state.[37] Annihilation of the largest contaminant and re-optimization of the position of the transition state along the reaction path yields a barrier of −0.9 kcal/mol at the PMP4/6-31G* level,[37] in very good agreement with experiment. Spin annihilation lowers the barrier for ethoxy decomposition by 6 kcal/mol. When the position of the transition state along the reaction path is re-optimized with spin annihilation, the barrier height is unchanged.[64] The calculated barrier, 18.2 kcal/mol, is in good agreement with the experimental values, 20 and 21.6 kcal/mol.[32–34]

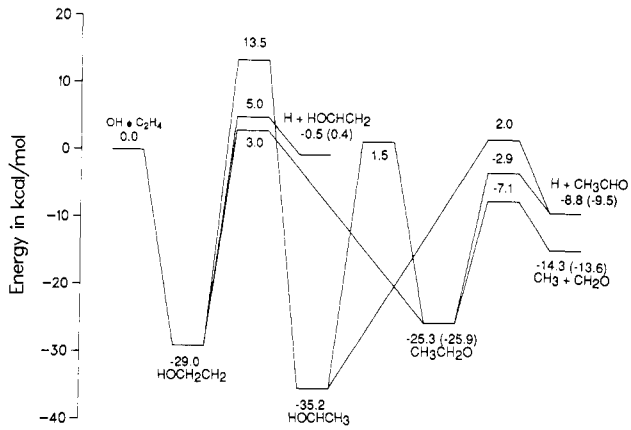

Figure 6. Theoretical estimates of the relative energies for the OH + C_2H_4 system.

Three of the reactions in Scheme I are [1,2]- or [1,3]-hydrogen shifts. The calculated barriers are 31.9 kcal/mol for $HOCH_2CH_2 \rightarrow OCH_2CH_3$, 42.5 kcal/mol for $HOCH_2CH_2 \rightarrow HOCHCH_3$, and 36.7 kcal/mol for $HOCHCH_3 \rightarrow OCH_2CH_3$ with spin projection at the UHF/6-31G* geometry. For an analogous reaction, $CH_3O \rightarrow CH_2OH$, re-optimization with spin projection and electron correlation changes the barrier by less than 0.3 kcal/mol.[69] Residual basis set effects can be significantly larger than this. A recent study of the [1,2]-hydrogen shift $CH_2O \rightarrow HCOH$ indicates that the barrier may be overestimated by as much as 6 kcal/mol at the MP4SDQ/6-31G** level, when compared to MP4SDTQ/6-311++G(3df,3pd) calculations.[68] If one assumes a similar error of 4–6 kcal/mol for radical [1,2] and [1,3] shifts, then better estimates for the barriers are 26–28, 36–38, and 31–33 kcal/mol, respectively. When combined with the corrected heats of reaction discussed above, this suggests that the [1,3]-shift transition state is comparable in energy to the OH + C_2H_4 transition state.

The barriers for [1,2]- and [1,3]-hydrogen shifts are typically 70–100 kcal/mol for closed-shell systems such as $CH_2O \rightarrow HCOH$ and $CH_3CHO \rightarrow HOCHCH_2$ but only 30–40 kcal/mol for the open-shell systems treated here. In the closed-shell examples, the barrier is due to a high energy avoided crossing between a doubly occupied HOMO and an empty LUMO. The lower barrier for the hydrogen shifts in $HOCH_2CH_2$, $HOCHCH_3$, and OCH_2CH_3 can be rationalized by considering the HOMO of the radicals to be half-filled. Hence, the radicals require only half the energy to surmount the barrier due to the avoided crossing between the HOMO and the LUMO.

The reverse of reactions IV, VII, and VIII in Scheme I are hydrogen atom additions to double bonds. The calculated barrier heights are 5.5 kcal/mol for H + $HOCHCH_2 \rightarrow HOCH_2CH_2$, 5.9 kcal/mol for H + $CH_3CHO \rightarrow CH_3CH_2O$, and 10.8 kcal/mol for H + $CH_3CHO \rightarrow HOCHCH_3$. Comparison with H + C_2H_2 suggests that re-optimization with spin projection will change these barriers by less than ±1 kcal/mol. Calculations on H + C_2H_3Cl indicate that addition to the unsubstituted carbon has a barrier almost identical to that of H + C_2H_4. Thus, a barrier of 2 kcal/mol can be estimated for H + $HOCHCH_2 \rightarrow HOCHCH_3$.

A summary of the energetics is given in Figure 6. The isodesmic reactions in Table IV have been used to lower the calculated energies of $HOCH_2CH_2$ and CH_3CHOH by 4.6 kcal/mol and $HOCHCH_2$ by 6.0 kcal/mol. The barrier heights in Table V were added to these adjusted energies to obtain the transition-state energies relative to OH + C_2H_4. The results agree very well with the BAC-MP4 calculations of Melius, Binkley, and Koszykowski.[48] Although quite different methods are used to

correct the MP4 calculations, the average difference in the relative energies is less than 2 kcal/mol. In $HOCH_2CH_2$, the barriers for the [1,3] shift to form ethoxy radical and for the loss of H to form vinyl alcohol are close in energy, but slightly higher than decomposition to HO + C_2H_4; the [1,2] shift is the least favorable reaction. The three lowest energy pathways for unimolecular decomposition of $HOCHCH_3$ are nearly equal in energy: isomerization to ethoxy radical, loss of H to form acetaldehyde, and loss of H to form vinyl alcohol (not shown, ca. 1.5 kcal/mol relative to OH + C_2H_4). The other [1,2]-shift transition state to form $HOCH_2CH_2$ is at least 10 kcal/mol higher. Decomposition of ethoxy radical occurs via loss of CH_3. The loss of H, the [1,2] shift, and the [1,3] shift require substantially more energy.

Acknowledgment. This work was supported by a grant from the National Science Foundation (Grant No. CHE-83-12505).

Registry No. HO•, 3352-57-6; C_2H_4, 74-85-1; $HOCH_2CH_2$•, 4422-54-2; CH_3CH_2O•, 2154-50-9; $HOCHCH_3$, 2348-46-1; CH_2=CHOH, 557-75-5; H, 12385-13-6; CH_2O, 50-00-0; CH_3•, 2229-07-4; CH_3CHO, 75-07-0.

Solid-State ^{13}C NMR Investigation of Methyltin(IV) Compounds. Correlation of NMR Parameters with Molecular Structure

Thomas P. Lockhart*[1] and William F. Manders[1]

Contribution from the National Bureau of Standards, Gaithersburg, Maryland 20899.
Received November 10, 1986

Abstract: Solid-state ^{13}C NMR data are reported for 52 methyltin(IV) compounds. The dependence of NMR parameters (chemical shift and tin–carbon J coupling, $|^1J(^{119}Sn,^{13}C)|$) on molecular structure has been investigated with reference to the X-ray structures known for many of the compounds. ^{13}C chemical shifts of the tin–methyls generally increase (are more deshielded) in the series tetra- < penta- < hexa- < heptacoordinated methyltin(IV) and tri- < di- < monomethyltin(IV) compounds, although there is considerable overlap between several of these groups. $|^1J(^{119}Sn,^{13}C)|$ values were determined for 29 compounds whose X-ray structures are known; a linear regression of the data for 28 compounds yields the equation $|^1J(^{119}Sn,^{13}C)| = 10.7$ (Me–Sn–Me angle) − 778 ($r = 0.975$). A Fermi contact term–tin hybridization model is used to rationalize the general behavior; changes in the effective nuclear charge of tin may be responsible for the several poorly behaved compounds that have been identified. Cases have been found in which more than one $|^1J(^{119}Sn,^{13}C)|$ value exists for the methyls in di- and trimethyltin(IV) compounds. This appears to arise in cases where the tin atom bonds to different methyls with substantially different hybrid orbitals.

We have suggested[2] that solid-state NMR provides a powerful means for discovering and for evaluating relationships between NMR and structural parameters. In a preliminary communication we reported[3] our finding that the magnitude of tin–carbon J coupling, $^1J(^{119}Sn,^{13}C)$ ($|^1J|$), measured for structurally characterized methyltin(IV) compounds by solid-state ^{13}C NMR, is linearly related to the Me–Sn–Me angle for di- and trimethyltin(IV)s. To account for this simple behavior we have offered a hypothesis that depends on the contribution of the Fermi contact term, FCT (commonly assumed to dominate J coupling interactions of organotin(IV) compounds), to $|^1J|$.[4–7] The FCT depends strongly on the s character of the bonding orbitals of the coupled nuclei, as should the Me–Sn–Me angle (larger angles in organotin(IV) compounds are believed[8] to reflect increased s character in the bonding orbitals); therefore, changes in the angle should be accompanied by corresponding changes in $|^1J|$.

The data for most methyltin(IV) compounds are well-behaved and the empirical $|^1J|$/angle relationship provides a useful tool for the structural analysis of uncharacterized methyltin(IV) compounds.[9,10] $|^1J|$ can also be determined for many methyltin(IV) polymers, and it provides one of the few probes of molecular structure for amorphous or microcrystalline methyltin(IV) compounds.[11] Because $|^1J|$ can be measured in solution, the solid-state NMR-derived relationship also can be used to estimate molecular structures in solution and to evaluate medium effects on the structure of methyltin(IV) compounds.[10,12]

Given the potential utility of the empirical relationship between $|^1J|$ and the Me–Sn–Me angle, it is important that its accuracy and limitations be broadly investigated. The physical basis for the simple empirical relationship is also of interest and, it is hoped, may be elucidated in part by the identification of compounds displaying exceptional behavior. In this paper we report solid-state ^{13}C NMR data for a large number of methyltin(IV) compounds. Data for several fall outside the simple relationship and raise interesting questions about the mechanism of tin–carbon J coupling in these molecules.

Results and Discussion

NMR of Methyltin(IV) Solids. Structure Correlations. Solid-state ^{13}C NMR data for 52 compounds are reported in Table I (along with solution data for Me_4Sn). For 41 of these compounds one or, usually, both of the tin–carbon J coupling satellites were visible and $|^1J|$ could be determined. The major difficulty encountered in observing the $^{117,119}Sn$ satellites and determining $|^1J|$

* Address correspondence to this author at ENIRICERCHE S.p.A., 20097 San Donato Milanese, Milano, Italy.

(1) National Bureau of Standards–National Research Council Postdoctoral Associate, 1983–1985.
(2) Manders, W. F.; Lockhart, T. P. *J. Organomet. Chem.* **1985**, *297*, 143.
(3) Lockhart, T. P.; Manders, W. F.; Zuckerman, J. J. *J. Am. Chem. Soc.* **1985**, *107*, 4546.
(4) De Poorter, B.; Gielen, M. *J. Organomet. Chem.* **1977**, *124*, 161.
(5) Steinborn, D.; Taube, R.; Radeglia, R. *J. Organomet. Chem.* **1982**, *229*, 159.
(6) Pyykko, P.; Wiesenfeld, L. *Mol. Phys.* **1981**, *43*, 557.
(7) Barbieri, G.; Benassi, R.; Taddei, F. *J. Organomet. Chem.* **1977**, *129*, 27. The percent of tin 5s orbital character is thought to be maximized in bonds to carbon and to increase as the Me–Sn–Me angle increases from 109.5° to 120° to 180° [as the hybridization of the tin orbitals directed toward carbon changes from sp^3 to sp^2 to sp (in *trans*-dimethyl octahedral complexes)].
(8) Okawara, R.; Wada, M. *Adv. Organomet. Chem.* **1967**, *5*, 144, 145. Tobias, R. S. *Organomet. Chem. Rev.* **1966**, *1*, 93.
(9) Lockhart, T. P.; Manders, W. F.; Schlemper, E. O. *J. Am. Chem. Soc.* **1985**, *107*, 7451.
(10) Lockhart, T. P.; Manders, W. F.; Holt, E. M. *J. Am. Chem. Soc.* **1986**, *108*, 6611.
(11) (a) Lockhart, T. P.; Manders, W. F. *J. Am. Chem. Soc.* **1985**, *107*, 5863. (b) Lockhart, T. P.; Manders, W. F. *Inorg. Chem.* **1986**, *25*, 1068.
(12) Lockhart, T. P.; Manders, W. F.; Schlemper, E. O.; Zuckerman, J. J. *J. Am. Chem. Soc.* **1986**, *108*, 4074.